Amplification of Ultrashort Laser Pulses by a Resonant Raman Scheme in a Gas-Jet Plasma

Yuan Ping, Weifeng Cheng, and Szymon Suckewer

School of Engineering and Applied Science, Department of MAE, Princeton University, Princeton, New Jersey 08544, USA

Daniel S. Clark and Nathaniel J. Fisch

Princeton Plasma Physics Laboratory, P.O. Box 451, Princeton, New Jersey 08543, USA

Raman amplification of subpicosecond laser pulses up to 95 times is demonstrated at corresponding frequencies in a gas-jet plasma. The larger amplification is accompanied by a broader bandwidth and shorter pulse duration. Theoretical simulations show a qualitative agreement with the measurements, and the effects of the plasma conditions and laser intensities are discussed.

Current ultrashort pulse lasers depend on the chirped-pulse-amplification (CPA) method [1]. This very successful method is limited at ultrahigh intensities mainly due to the damage threshold of gratings in the final compressor. The amplification and compression of laser pulses in the plasma have been proposed [2–4] in order to overcome this limit, since plasma has no thermal damage threshold. Of particular interest is a transient Raman scheme [3], in which a short seed pulse is amplified by a counterpropagating long pumping pulse when their frequencies satisfy the relation $\omega_{\text{seed}} = \omega_{\text{pump}} - \omega_p$, where ω_p is the plasma wave frequency ($\omega_p^2 = 4\pi e^2 n_e / m_e$; n_e is the plasma electron density, and m_e is the electron mass). In the linear regime of the Raman scheme, pump depletion is negligible, and the seed pulse is amplified and lengthened due to the narrow bandwidth of linear amplification (which is approximately twice the growth rate [5]). In the nonlinear regime, significant pump depletion takes place, and simultaneous compression of the amplified pulse is possible, since the front of the pulse is amplified while the tail part interacts with a depleted pump and is not pumped as strongly as the front [6]. Such a scheme is of interest in fast ignition for inertial confinement fusion [7], laser wakefield accelerator [8], x-ray lasers [9], etc., due to its potential of generating ultraintense laser pulses.

In our recent papers [10–12], we presented the first experimental results on this novel Raman scheme. An amplification of up to eight was obtained in microcapillary plasmas ($n_e \approx 1.1 \times 10^{20}$ cm^{-3}) and ~ 2 in a gas-jet plasma ($n_e \approx 1.3 \times 10^{19}$ cm^{-3}). The modest amplification was due mainly to the plasma density inhomogeneity. In order to obtain larger amplification, we improved the experiment by enhancing the seed intensity, refining the spatial and temporal overlap between the seed and pump, and improving the axial uniformity of the plasma density. In this Letter we report an amplification close to 100 at corresponding Raman frequencies in the gas-jet plasma. This indicates the practical possibility for ultrashort pulse amplification in plasma. Theoretical modeling shows a qualitative agreement with the measurements and illustrates the effects of laser intensities and the plasma conditions on the amplification process.

The experimental setup was similar to that in Ref. [12]. The 800 nm laser pulse was split into two parts: one (80% energy) was compressed to ~ 10 ps, while preserving the original bandwidth (~ 11 nm) to serve as the pumping pulse; the other (20% energy) was compressed to ~ 500 fs and then frequency doubled by a beta barium borate crystal to pump an optical parametric generator [13] and generate the seed pulse. The seed spectrum was broadband, spreading from 840 to 940 nm, which covered a density range of 0.4–3.8×10^{19} cm^{-3}. The pump and the seed pulses were focused to the center of the plasma from opposite directions. The focal spots of the pump and the seed were measured to be both ~ 30 μm (FWHM) for $f/15$ lenses. The Rayleigh lengths were ~ 1 mm for both beams, which was longer than the density scale length. The energies were 15–20 mJ for the 10-ps pump and 5–8 μJ for the 500-fs seed, resulting in vacuum intensities of 1.5×10^{14} and 1.5×10^{12} W/cm^2, respectively. The effective seed intensity was $\sim 1.5 \times 10^{11}$ W/cm^2 since only 10% of the spectral width was in resonance when amplified. The synchronization of the pump and seed pulses with a precision of 0.5 ps was accomplished by scanning an optical delay line to maximize the amplification. This scan showed a synchronization window whose width was similar to the duration of the pump. Because of the shot-to-shot fluctuation of the plasma density, it was not possible to observe the effect of the pump chirping.

The plasma was created in a C_3H_8 gas jet (orifice 0.5×2 mm) through optical breakdown by another low-power laser pulse (called the prepulse, ~ 400 mJ in 7 ns at 1.06 μm, focused to a 50-μm spot by a $f/20$ lens). The plasma density was varied by adjusting the delay between the prepulse and the other two pulses and was measured interferometrically by a probing beam passing through the plasma transversely, showing a density plateau $\gtrsim 0.5$ mm at a delay of 20–30 ns. A small portion of

the seed pulse was split out and sent to the spectrometer directly, providing a reference spectrum. The entrance slit of the spectrometer was 100 μm for a spectral resolution of 0.3 nm. The amplification was calculated as the ratio of the amplified pulse spectrum to the reference spectrum. The transmitted spectrum was attenuated by neutral density filters so that its ratio to the reference spectrum fell within 1.0 ± 0.2 when the plasma and the pump were absent. We did not observe any significant change in this ratio for nonresonant wavelengths when the plasma and the pump were present.

A typical spectrum of the amplified pulse is shown in Fig. 1(a), together with the reference spectrum. The bright spot in the amplified pulse spectrum corresponds to the Raman resonance. Accordingly, the intensity profile displays a peak, as shown in Fig. 1(b) (solid line), in contrast to the reference spectrum (dotted line). The ratio of these two spectra, shown in Fig. 1(c), demonstrates an amplification of ~ 10, near $\lambda = 865$ nm, which corresponds to $n_e \simeq 1.0 \times 10^{19}$ cm^{-3}. This density was deduced from thermal Raman backscattering (RBS, originated from thermal noise) at a higher pumping intensity without the seed pulse, which also agreed well with interferometric measurements. For all measurements of the amplification, the pumping intensity was kept below the threshold of the thermal RBS so that there was no signal in the spectrum without the seed pulse.

The amplifications at four delays (and hence four different densities) are shown in Fig. 2. At 10 ns after the prepulse, the plasma density is higher, and therefore the resonance peak occurs at a longer wavelength, $\lambda = $ 888 nm (corresponding to $n_e \simeq 1.7 \times 10^{19}$ cm^{-3}). As the delay increases, the plasma density decreases, resulting in the shift of the resonance peak toward shorter wavelengths. As one can see in Figs. 2(b)–2(d), the resonance takes place at 873 nm ($n_e \simeq 1.2 \times 10^{19}$cm^{-3}) for delay 15 ns, at 860 nm for delay 20 ns ($n_e \simeq 0.9 \times 10^{19}$ cm^{-3}) and at 855 nm for delay 30 ns ($n_e \simeq 0.7 \times 10^{19}$ cm^{-3}). At the delay of 20 ns, the measured amplification exceeds 90. The variation of the amplification at different delays can be roughly explained by its dependence on the density and the effective plasma length L_p. In the linear regime, the pulse grows as $\exp(2\gamma_{RBS}L_p/c)$, where $\gamma_{RBS} = a_{pump}(\omega_{pump}\omega_p/4)^{1/2}$ is the linear growth rate [$a_{pump} \simeq 8.5 \times 10^{-10}\lambda_{pump}(\mu m)I_{pump}^{1/2}(W/cm^2)$ is the normalized vector potential]. Therefore, at the same I_{pump}, the exponent scales as $n_e^{1/4}L_p$. At short delays, n_e is higher, but the interaction length is very short, while at much longer delays, there is a drop in n_e, and L_p may also decrease due to recombination, both leading to smaller amplifications. The product $n_e^{1/4}L_p$, hence the amplification, usually reaches a maximum at around 20 ns.

It is interesting to note that in Fig. 2 the spectral bandwidth of the pulse with higher amplification [Fig. 2(c)] is larger than that with lower amplification [Figs. 2(a), 2(b), and 2(d)]. The bandwidth (FWHM) as a function of the amplification is plotted in Fig. 3. Despite the large fluctuation in the data, a trend can be seen showing that the bandwidth increases for larger amplifications. The density for each data point is also shown in Fig. 3, indicating that the bandwidth is correlated not with the density but with the amplification. For example, at the same delay of 20 ns (hence at approximately the same n_e), when the pulse has an amplification of ~ 90, its FWHM is ~ 7 nm, whereas at an amplification ~ 10 its FWHM is $\sim 2–3$ nm
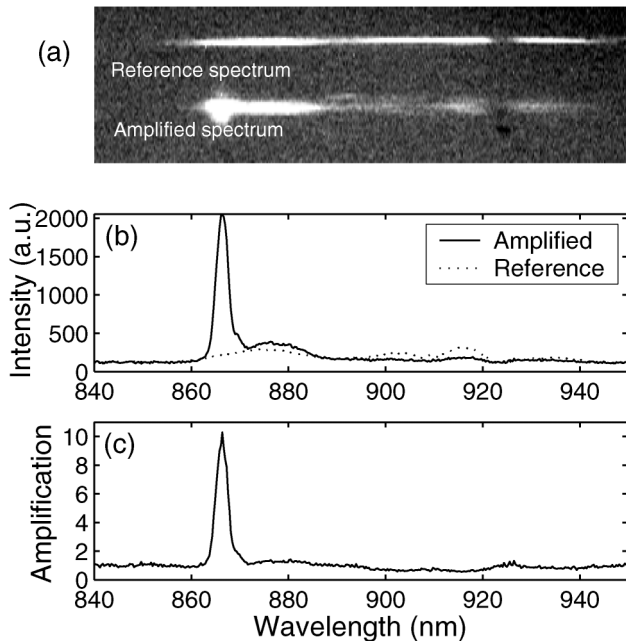
FIG. 1. (a) Spectra of the reference and the amplified pulse. (b) Intensity versus wavelength for the reference (dotted line) and the amplified pulse (solid line). (c) Ratio of the two spectra, demonstrating an amplification of ~ 10.
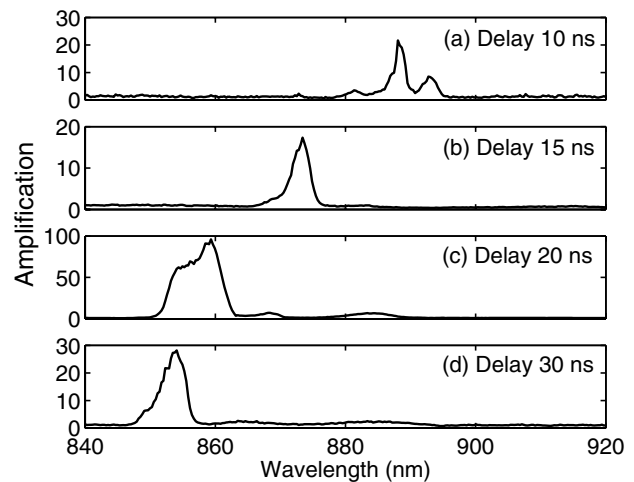
FIG. 2. The amplifications at four delays, showing the shift of the resonance wavelength at various densities. (a) Delay 10 ns ($n_e \simeq 1.7 \times 10^{19}$ cm^{-3}). (b) Delay 15 ns ($n_e \simeq 1.2 \times 10^{19}$ cm^{-3}). (c) Delay 20 ns ($n_e \simeq 0.9 \times 10^{19}$ cm^{-3}). (d) Delay 30 ns ($n_e \simeq 0.7 \times 10^{19}$cm^{-3}). The maximum amplification is ~ 95.
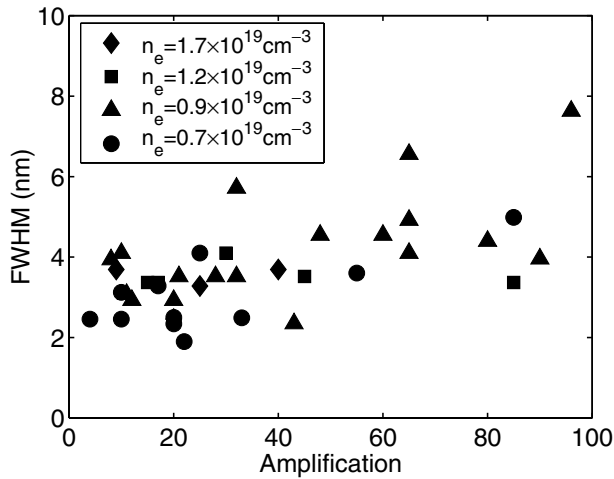
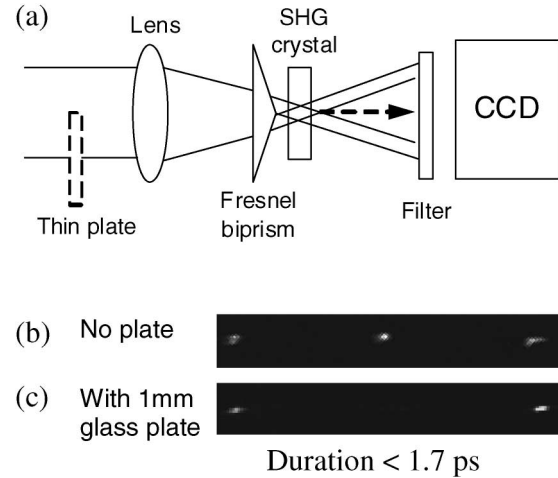FIG. 3. FWHM of the amplified pulse versus amplification.

FIG. 4. (a) Setup of the simplified autocorrelator for the pulse duration measurements. (b) CCD image of the second harmonics with no plate inserted. (c) CCD image with a 1-mm glass plate.

[see Fig. 1(c)]. The FWHM of thermal RBS was found to be ~3 nm at a twice higher pumping intensity. When the amplification is below ten, the FWHM of the amplified pulse (2.5 nm) is similar to that of the thermal RBS, and it rises up to 7.5 nm for the largest amplification. The small bandwidth (2.5 nm) agrees well with the linear growth rate ($\Delta\omega \sim 2\gamma_{RBS}$). The large increase in the bandwidth cannot be solely explained by higher local growth rates because otherwise the factor-of-three broadening would indicate a 9-fold increase in I_{pump} or an 81-fold increase in n_e ($\Delta\omega \propto \gamma_{RBS} \propto I_{pump}^{1/2} n_e^{1/4}$), which are both very unlikely.

The duration of the amplified pulse was a key measurement for clarification of the spectral broadening issue. In the linear regime, in the absence of damping, one expects lengthening of the pulse; in the nonlinear pump depletion regime, one expects shortening. However, the seed pulse was too weak to measure the duration directly with our commercial autocorrelator. Therefore, we employed a "single point" autocorrelator, which provided the upper limit of the pulse duration. The setup of this autocorrelator is shown in Fig. 4(a). The beam was focused by a lens onto a beta barium borate crystal to generate the second harmonic. A Fresnel biprism [14] was placed between the lens and the second-harmonic generation (SHG) crystal so that the beam was split into two parts. The crystal was located in the overlap region of the two beams. Without any other optics, these two beams were synchronized inside the crystal and generated a second harmonic at the center (indicated by the arrow). The beams themselves could also generate second harmonics, which propagated along with them. Therefore, three points appeared in the charge-coupled device (CCD) image (the fundamental frequencies were blocked by a filter), as shown in Fig. 4(b). The central point was the second harmonic from both beams, and the two side points were the second harmonics of each beam by itself (self-harmonics). If a thin plate was inserted into half of the incident beam, a temporal delay was introduced be-

tween the two split beams. If the plate was thick enough to temporally separate the two beams in the crystal, the second harmonic at the center would disappear, as shown in Fig. 4(c), while the self-harmonics were still present. The appearance of the self-harmonics ensured that the intensity of the beam was high enough to generate the second harmonic. Therefore, the disappearance of the central point was only due to the temporal delay induced by the plate. In the case of Fig. 4(c), the central point disappeared when a 1-mm glass plate was inserted, leading to the conclusion that the seed pulse was shorter than 1.7 ps. In fact, by scanning the delay line in the optical parametric generator, it was found out that the duration of the initial seed pulse was 400–500 fs (FWHM).

To check the pulse duration and its correlation with the amplification, a portion of the amplified pulse was split out before entering the spectrometer and aligned into the single point autocorrelator so that the amplification and the pulse duration measurements could be carried out simultaneously. When the amplification was relatively low (~5), there were three points in the SHG image with a 1.5-mm glass plate, showing that the pulse was longer than 2.5 ps. Since the initial seed pulse was only about 400–500 fs long, this indicates the lengthening of the amplified pulse in the linear regime. Without the glass plate, all three points, especially the central one, brightened strongly with a large amplification (additional neutral density filters were added to avoid saturation of the camera). When the glass plate was inserted, the central point in the SHG image disappeared as the amplification reached over 20, indicating that the amplified pulse became shorter than 2.5 ps. It would be very important if this indicated the onset of the pulse shortening associated with the nonlinear regime; however, there are explanations of this shortening possible within the linear regime as well, once damping is taken into account [15].

To understand these observations we performed 1D modeling using the F3D code [16]. The calculations were run for $n_e = 1.0 \times 10^{19}$ cm^{-3} and a 500-fs square-shaped seed pulse. Some results of the amplification (I_{out}/I_{seed}) and the pulse duration (calculated at 5% of maximum) versus plasma length are plotted in Figs. 5(a) and 5(b), respectively, for various intensities and electron temperature T_e. The simulations show that at $I_{pump} = 1.0 \times 10^{14}$ W/cm^2, $I_{seed} = 1.0 \times 10^{11}$ W/cm^2 and $T_e = 10$–80 eV, an amplification of 100 is achievable for $L_p \sim 0.5$ mm (the solid line is for $T_e = 25$ eV). This reasonably agrees with the experiment. Figure 5(b) shows that at these parameters the pulse duration lengthens to ~ 2 ps until the onset of the nonlinear regime at $L_p \sim 0.8$ mm, where the amplification turns from an exponential growth to a linear growth. One can also see that a mild increase in L_p by 0.2 mm can lead to an order of magnitude enhancement in the amplification. Thus it is important to extend the effective plasma length, or in other words, to improve the uniformity. The effect of T_e on the amplification is generally governed by collisional damping (at $T_e < 5$ eV) and Landau damping (at $T_e > 100$ eV) of the waves [15]. Therefore, there is a temperature window to obtain large amplification. As indicated by the dashed line in Fig. 5, the strong Landau damping of the plasma wave at $T_e = 100$ eV lowers the gain, and the nonlinear regime is not reached even at the maximum simulated length $L_p = 1.6$ mm. The simulations also indicate that a higher pumping intensity does not necessarily result in better amplification because the thermal RBS can outgrow the amplified pulse. The dot-dashed line in Fig. 5 is for a slightly higher I_{pump} (1.5 $\times 10^{14}$ W/cm^2). The $T_e = 75$ eV is chosen to be high enough to suppress the thermal RBS, but not too high to damp the amplification. In this case, the amplification grows faster, as expected, but the pulse is not compressed as well as in the first case. Another approach to improve the amplification is to increase I_{seed}. As shown by the dotted line ($I_{seed} = 1.0 \times 10^{12}$ W/cm^2), the pump is quickly depleted, and the onset of the nonlinear regime occurs at a shorter length ($L_p = 0.6$ mm). The amplified pulse is compressed back to its original duration at $L_p = 1.6$ mm. The FWHM of the final pulse is actually only ~ 150 fs, and the output intensity exceeds the pumping intensity by an order of magnitude. These simulations provide a guide for future experiments on the Raman scheme.

To summarize, we have demonstrated an amplification up to ~ 95 for short laser pulses via the resonant Raman scheme in a gas-jet plasma. At various plasma densities, the Raman resonance takes place at the corresponding wavelength. The observed bandwidth of the amplified pulse increases with the amplification. Pulse duration measurements with a single point autocorrelator show that shorter output pulses are correlated with larger amplification. In this experiment, the seed was chosen to be broadband in order to demonstrate resonances at different
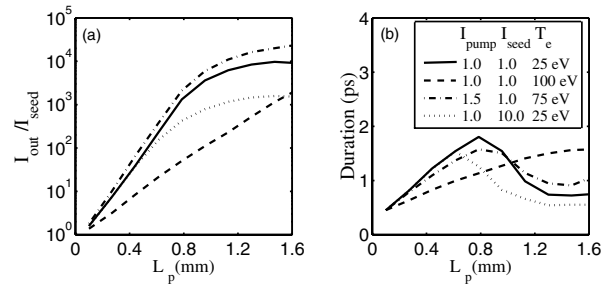

FIG. 5. Simulation results: the amplification (I_{out}/I_{seed}) (a) and the pulse duration (b) as a function of the plasma length L_p. I_{pump} is in 10^{14} W/cm^2, I_{seed} is in 10^{11} W/cm^2, and $n_e = 1.0 \times 10^{19}$ cm^{-3}.

densities. If the broadband seed is replaced by a narrow-band one at the resonant wavelength, the factor of 95 would be the whole energy gain. Although these measurements do not yet confirm the onset of the nonlinear depletion regime, the very large amplification is a significant step towards achieving that regime and ultimately a practical scheme for amplification of ultrashort laser pulses.

[1] M. D. Perry and G. Mourou, Science **264**, 917 (1994).
[2] G. Shvets, N. J. Fisch, A. Pukhov, and J. MeyerterVehn, Phys. Rev. Lett. **81**, 4879 (1998).
[3] V. M. Malkin, G. Shvets, and N. J. Fisch, Phys. Rev. Lett. **82**, 4448 (1999).
[4] D. S. Clark and N. J. Fisch, Phys. Plasmas **9**, 2772 (2002).
[5] C. B. Darrow et al., Phys. Rev. Lett. **69**, 442 (1992).
[6] N. J. Fisch and V. Malkin, Phys. Plasmas **10**, 2056 (2003).
[7] M. Tabak et al., Phys. Plasmas **1**, 1626 (1994).
[8] P. Sprangle, E. Esarey, J. Krall, and G. Joyce, Phys. Rev. Lett. **69**, 2200 (1992).
[9] J. Dunn et al., Phys. Rev. Lett. **84**, 4834 (2000).
[10] Y. Ping, I. Geltner, N. J. Fisch, G. Shvets, and S. Suckewer, Phys. Rev. E **62**, R4532 (2000).
[11] Y. Ping, I. Geltner, A. Morozov, N. J. Fisch, and S. Suckewer, Phys. Rev. E **66**, 046401 (2002).
[12] Y. Ping, I. Geltner, and S. Suckewer, Phys. Rev. E **67**, 016401 (2003).
[13] J. Zhang, Z. Yu, Y. Kong, C. Yu, and Y. Wu, Appl. Opt. **37**, 3299 (1998).
[14] P. O'Shea, M. Kimmel, X. Gun, and R. Trebino, Opt. Lett. **26**, 932 (2001).
[15] D. S. Clark and N. J. Fisch, Phys. Plasmas **10**, 3363 (2003).
[16] R. L. Berger, C. H. Still, E. A. Williams, and A. B. Langdon, Phys. Plasmas **5**, 4337 (1998).